THE JOURNAL OF PHYSICAL CHEMISTRY B

Article

pubs.acs.org/JPCB

Origins of Spectral Broadening in Iodated Vaska's Complex in Binary Solvent Mixtures

Brynna H. Jones and Aaron M. Massari*

Department of Chemistry, University of Minnesota—Twin Cities, 207 Pleasant Street Southeast, Minneapolis, Minnesota 55455, United States

Supporting Information

ABSTRACT: Linear absorption spectroscopy of the iridium-bound carbonyl on an iodated adduct of Vaska's complex has shown that the mean vibrational frequency is insensitive to solvation by a broad range of solvents, while the spectral line width changes significantly. The spectral broadening is more significant in chloroform than benzyl alcohol, which is puzzling considering that benzyl alcohol is more polar. In this study, 2D-IR spectroscopy was performed on this vibrational mode to dissect the linear line shape into its homogeneous and inhomogeneous contributions in binary solvent mixtures of either chloroform or benzyl alcohol in d_6-benzene. The full frequency−frequency correlation function was determined, including the homogeneous line width and fast spectral diffusion. We find that the frequency fluctuation magnitudes show the most notable changes in chloroform mixtures, while the time constants for spectral diffusion change more dramatically in benzyl alcohol mixtures. Nonetheless, we conclude that the frequency fluctuation magnitudes in both solvent mixtures most clearly explain the differences in their linear line widths. The homogeneous contributions were found to either stay the same or decrease as the more polar solvent was added to d_6-benzene, thereby implicating inhomogeneous dynamics as the dominant broadening mechanism.

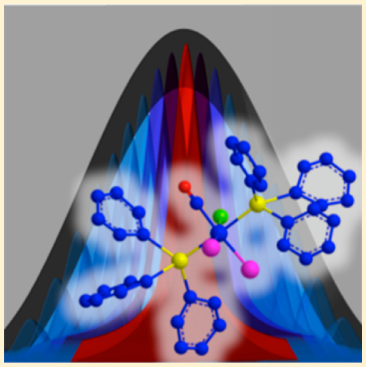

INTRODUCTION

Although it is often the average peak frequency that is used in vibrational analyses, there is a wealth of information contained in spectral line shapes that is lost in linear spectroscopy, particularly the dynamic interactions of the solvation shell molecules with the solute of interest. In the condensed phase, the linear line shape can be considered as a heterogeneous collection of subensembles, each of which characterizes a particular solvent−solute configuration (see Figure 1). This inhomogeneous distribution is often well-approximated by a Gaussian line shape whose width is notably larger than any of the underlying ensembles and describes the full range of solvent−solute configurations in the sample. These chemical microstates are dynamic; they have the potential to change their mean frequencies as solvent−solute configurations interconvert over a continuum of time scales. These time scales may be measurable as spectral diffusion or appear to be static for a given technique. The contributions to the individual subensemble line widths (Γ) are also dynamic, being dictated by pure dephasing (T_2^*), population relaxation (T_1), and solute reorientation (T_{orient}) according to[1−4]

$$\Gamma = \frac{1}{\pi T_2} = \frac{1}{\pi T_2^*} + \frac{1}{2\pi T_1} + \frac{1}{3\pi T_{orient}} \quad (1)$$

Hence, the overall FTIR line width is a combination of inhomogeneous and homogeneous broadening phenomena, both of which are dynamic yet appear to be static through the lens of the FTIR measurement.

The convolution of inhomogeneous and homogeneous broadening contributions means that all of the dynamic solvent−solute interactions beneath the FTIR line shape are indistinguishable. Fortunately, nonlinear IR spectroscopy can be used to recover this information. The T_1 and T_{orient} times can be measured directly by polarization-controlled IR pump−probe spectroscopy to reveal the mechanisms of energy relaxation and the role of the solvation environment in facilitating or inhibiting molecular rotation.[5,6] T_2^* can be quantified by two-dimensional IR (2D-IR) spectroscopy to

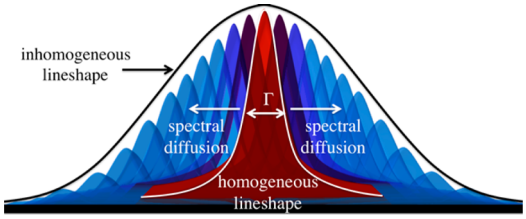

Figure 1. Diagram of an inhomogeneously broadened FTIR (linear) line shape composed of numerous homogeneous (blue and red) subensembles, each representing a solvent−solute configuration. The configurations have a homogeneous line width (Γ) and may spectrally diffuse to other mean frequencies as configurations interchange.

Special Issue: Michael D. Fayer Festschrift

Received: June 30, 2013
Revised: August 29, 2013

   dx.doi.org/10.1021/jp4064627 | J. Phys. Chem. B XXXX, XXX, XXX−XXX

determine the time scales on which the vibrational frequencies are modulated by their surrounding environments without relaxation.[7−13] In addition, this technique can be used to characterize the inhomogeneous dynamics of spectral diffusion, allowing full characterization of the origins of spectral broadening for a vibrational mode.[1,2]

In this study, we use 2D-IR spectroscopy,[7−13] as well as IR pump−probe results from a previous report,[14] to explore the origins of spectral broadening for a metal-bound CO vibrational mode across two binary solvent mixtures. The solute of interest is bis(triphenylphosphine) iridium(I) carbonyl chloride, or Vaska's complex (VC),[15−17] that has been converted to the iodated adduct by oxidative addition of iodine (VC-I_2).[18]

VC is an organometallic catalyst best known for its ability to reversibly bind and release oxygen, making it a model system for biomimetic oxygen transport.[15,19,20] It has also been shown to reversibly bind molecular hydrogen[16,21] but irreversibly add iodine[18] and to serve as an efficient catalyst for a number of chemical reactions following oxidative addition of the substrate.[19,21−28] The carbonyl ligand on VC adducts is trans to the bound addend and is sensitive to the oxidation state of the iridium[29,30] and also to the nature of the addend itself.[8,31] VC-I_2 presents an interesting case in which the average vibrational frequency of the CO is unchanged for a broad range of solvents, indicating that the oxidation state of the metal is nearly constant, yet the spectral line width changes dramatically.[14,31]

As stated above, nonlinear IR techniques can be used to separate the relative contributions to FTIR spectral broadening and will be used here to characterize the broadening influences for the CO on VC-I_2. Binary solvent mixtures of chloroform ($CHCl_3$) and benzyl alcohol (BA) in d_6-benzene were selected as two cases in which the extremes of spectral broadening were observed and a variety of solvent−solute interactions were present. By mapping the dynamical contributions to the line shape onto a coordinate in which the bulk solvent composition was varied linearly, we were able to test for preferential solvation dynamics of the solute within the first solvent shell. Solvation dynamics studies have also shown that binary solvent mixtures may have dynamical processes that are distinct from either of the pure solvents.[32−34] Such nonadditive behavior can be valuable when attempting to use solvation interactions to tune the response of a solute.[35−41] By combining these results with our previous measurements of the linear spectroscopic changes and the vibrational lifetime of this mode, we are able to provide a complete picture of the factors that lead to spectral broadening for the carbonyl on VC-I_2 in these solvent mixtures.

EXPERIMENTAL METHODS

Bis(triphenylphosphine) iridium(I) carbonyl chloride, (VC, 99.99%, Sigma Aldrich), chloroform ($CHCl_3$, 99.8%, Sigma Aldrich), benzyl alcohol (BA, ≥99%, Sigma Aldrich), perdeuterated (d_6-)benzene (99.5% D, Cambridge Isotope Laboratories, Inc.), and iodine (99.8%, Fisher Scientific) were used as received.

VC-I_2 solutions were prepared by dissolving 6 mg of VC with 2 mg of iodine in 2 mL of solvent. These solutions were first capped and parafilmed and then sonicated for at least 1 h in a water bath. All solutions were filtered through a 0.2 μm syringe filter before being placed in the sample cell. Typical VC concentrations were 4 mM. Solutions were used within 9 days of preparation. Solutions of the mixed solvents were stored in small vials with minimal headspace to reduce possible solvent composition changes due to evaporation. The sample cell had a path length of 150 μm.

Infrared spectra were collected on a Nicolet 6700 FTIR spectrometer (Thermo Scientific) with at least 16 scans and a typical resolution of 1 cm^{-1}. IR pump−probe spectra were collected for all samples in a previous study and were used for phase corrections to the 2D-IR data.[14,42]

The laser system used for 2D-IR and pump−probe spectroscopy has been described previously.[8] Briefly, a regeneratively amplified Ti:Sapphire laser (Spectra-Physics, 800 nm, 40 fs pulse duration full width at half-maximum (FWHM), 30 nm bandwidth FWHM, 600 mW) was used to pump an optical parametric amplifier (OPA) (Spectra-Physics) at a repetition rate of 1 kHz. The near-IR signal and idler beams generated by a β-barium borate (BBO, 3 mm thick) crystal in the OPA were difference frequency mixed in a silver gallium sulfide crystal ($AgGaS_2$, 0.5 mm thick) to generate 3 μJ mid-IR pulses. The mid-IR spectrum of the final output pulses was centered at the iridium-bound CO symmetric stretching frequency in VC-I_2 with approximately 200 cm^{-1} of bandwidth (FWHM). The pulses had a temporal duration of 90 fs FWHM (~1.2 times the transform limit) as measured by three-pulse cross-correlation using the nonresonant third-order signal from a 50 μm thick carbon tetrachloride cell.

The 2D-IR spectrometer has been described in detail elsewhere and will only briefly be detailed here.[8] The 2D-IR pulse sequence consisted of three ~1 μJ p-polarized mid-IR pulses in a BOXCARS geometry.[43] The generated vibrational echo signal was spatially coaligned with a local oscillator reference pulse (0.3−0.5 nJ per pulse, approximately 100× larger than the signal), spectrally resolved in a 0.32 m monochromator with a 75 line/mm grating, and detected with a liquid-N_2-cooled 64-element mercury cadmium telluride (MCT) linear array detector (Infrared Associates, Inc.). The spectral resolution of the detection system was ~4 cm^{-1}. The entire optical system was purged with dry air (−100 °F dewpoint) during data collection.

In a 2D-IR measurement, the first frequency dimension (ω_m) was achieved by optical Fourier transform of the heterodyne-detected vibrational echo signal by dispersing it from the monochromator diffraction grating.[44−47] For the second dimension (ω_τ), the time delay between pulses 1 and 2, τ, was scanned in increments of 5 fs and subsequently Fourier-transformed. Each spectrum was taken while the time delay between pulses 2 and 3, T_w, was maintained at a fixed value. Beam 3 was chopped at 500 Hz, and the chopped signal was divided by the laser spectrum to account for the laser power differences across the range of frequencies examined. The 2D-IR data were collected over a sufficiently large τ range, that the signal had decayed to zero in both the rephasing and nonrephasing scan directions; hence, no apodization or windowing functions were applied to the data. The purely absorptive 2D-IR spectrum was found using the technique described by Khalil and co-workers.[9,48] In order to account for systematic and random errors in the instrumentation, the data were then phase processed, as described in detail by others.[2,49] The pump−probe projection theorem and absolute value center method were used as constraints during this procedure.[42] The resulting data plots were then analyzed using the center line slope (CLS) procedure developed by Kwak and co-workers in order to extract the frequency−frequency correlation function (FFCF) from the 2D-IR data directly, as described in more detail below.[1,2]

dx.doi.org/10.1021/jp4064627 | J. Phys. Chem. B XXXX, XXX, XXX−XXX

RESULTS AND DISCUSSION

The frequency of the carbonyl stretch on VC-I_2 is effectively invariant to solvent composition for a wide range of solvents, including the three studied here.[14,31] In contrast, the FTIR line width changes significantly as the bulk solvent composition is varied linearly in binary mixtures of either $CHCl_3$ or BA in d_6-benzene.[14,31] Herein, we define the solvent composition by the mole fraction metric, but we have also considered the data as a function of volume fraction and found the observed trends to be the same. Figure 2 shows the FWHM values for the CO

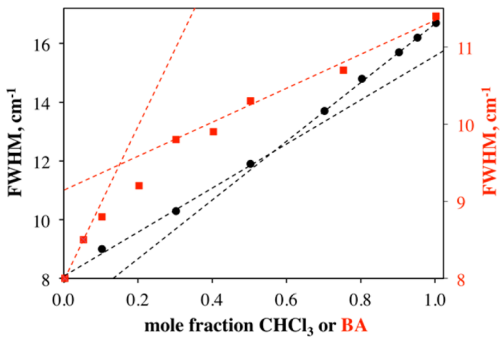

Figure 2. The FWHM for the linear line shapes of the CO on VC-I_2 in binary solvent mixtures of $CHCl_3$ (black circles) and BA (red squares) in d_6-benzene. Dashed lines are linear regression fits to the first or last points.

vibration on VC-I_2 as a function of the mole fraction of $CHCl_3$ (black circles) and BA (red squares). The full linear spectra are available in previous publications.[14,31] The change in spectral width is most drastic in the $CHCl_3$/d_6-benzene mixtures, varying monotonically and in a mostly linear fashion from 8 cm^{-1} in pure d_6-benzene to nearly 17 cm^{-1} in pure $CHCl_3$.[14] A linear variation of a spectral variable with the solvent mole fraction would indicate that the static and dynamic influences of the solvation shell(s) on the carbonyl frequency change in a proportional manner. This does not imply that the solvent shell composition is the same as the bulk solvent mixture, which it likely is not, but simply that it changes uniformly as the bulk composition is varied. If nonlinear behavior is observed, this is interpreted as preferential solvation in which the solvent shell composition and/or dynamics are more heavily dominated by one solvent over the other.[32−34,50,51]

A closer examination of the $CHCl_3$ data in Figure 2 reveals a slight variation in slope when only the first or last three points are fit to a line. The bulk composition of the surrounding solvent is changing linearly, but the influence on the line width is not perfectly linear over the entire range. We see that the broadening is slower (lower slope) at solvent compositions that have a majority of d_6-benzene than those that have a majority of $CHCl_3$. Whatever the underlying origins are for carbonyl FTIR line shape broadening, which is the subject of this paper, they are preferentially affected by d_6-benzene over $CHCl_3$ and require higher bulk concentrations of $CHCl_3$ before the influence of this secondary solvent dominates. Using the point at which the trend lines cross, we can say that between 0.5 and 0.6 mol fractions of $CHCl_3$, the line width trend begins to converge on the neat chloroform FWHM. Although the total broadening is smaller for the carbonyl vibration in BA mixtures in Figure 2 (note the different y-axis scale), it is more clearly nonlinear, indicating preferential solvation of VC-I_2 by this solvent over d_6-benzene. The low and high mole fraction trend lines cross between 0.1 and 0.2 mol fractions, and the low mole fraction line has the higher slope, indicating that a small amount of BA has a disproportionately large influence on the FTIR line width over d_6-benzene.

Understanding the reasons for the nonlinear evolution of the CO line width for VC-I_2 is the purpose of this study. As mentioned above, the dynamical variables that contribute to the spectral line widths are T_2^*, T_1, and T_{orient}, and we can directly quantify these contributions with IR pump−probe and 2D-IR spectroscopies. We have previously reported the vibrational lifetimes for this complex in the $CHCl_3$ and BA binary mixtures with d_6-benzene.[14] It was shown that T_1 increases linearly in $CHCl_3$ but *decreases* linearly in BA, despite the fact that both show an increase in the overall line width (see Figure 2), indicating that some other factor is the likely cause of this broadening. In addition, the T_1 values for the VC-I_2 carbonyl in these solvents are so long that their contribution to the overall line shape is comparatively miniscule. For example, the vibrational lifetimes in neat d_6-benzene, $CHCl_3$, and BA are 193, 216, and 124 ps, respectively, which contribute 0.03, 0.02, and 0.04 cm^{-1} to the homogeneous line width. On the basis of its molecular size, we can estimate that T_{orient} is on the order of hundreds of ps. Similarly sized complexes were reported to have rotational times of 150−400 ps in solvents of similar viscosity to those used in this study, also giving a small line width contribution of 0.02−0.009 cm^{-1}.[52,53] This number would be similar in all solvent mixtures because the solute is the same throughout these studies. Moving forward, we conclude that the contributions of T_1 and T_{orient} to the homogeneous line shape are negligible and focus our attention on determining the time scales of T_2^* and spectral diffusion as measured by 2D-IR spectroscopy. As we will show below, this approximation is justified because these two terms contribute only a few percent of the homogeneous line width.

Representative 2D-IR plots give qualitative insight into the dynamics present in these systems. The 2D-IR spectra for every T_w measured for all binary solvent mixtures are provided in the Supporting Information. Figure 3 shows the 2D-IR spectra at a short (0.3 ps, top row) and a long (30 ps, bottom row) T_w for each of the three neat solvents and their corresponding 0.5 mol fraction mixtures. A 2D-IR spectrum is a frequency correlation plot for the subensembles beneath the FTIR line shape.[7−13] The red positive-going peaks show the bleached $\nu = 0$ to 1 transition, while the blue negative-going peaks are the $\nu = 1$ to 2 vibrational excited-state absorptions that are shifted by the anharmonicity to lower frequencies. Assuming sufficient separation between the 0−1 and 1−2 peaks, the projection of a diagonal slice through the 0−1 peak onto either axis reflects the linear line shape, which is of course more easily obtained from a FTIR measurement. However, new information is obtained along the antidiagonal dimension of the 2D-IR spectrum. In the absence of spectral diffusion of oscillators from one solvent configuration to another, the antidiagonal width reports the homogeneous line shape. In most cases, interconversion of molecular subensembles driven by the reorganization of solvent molecules in the first few solvation shells leads to broadening along the antidiagonal dimension as T_w increases. Even at short T_w's (top row, Figure 3), presumably some spectral diffusion has occurred, and an antidiagonal slice is already broader than the homogeneous line width. After describing the qualitative features of the 2D-IR spectra below, CLS decay analysis will be used to quantitatively characterize the homogeneous and inhomogeneous contribu-

dx.doi.org/10.1021/jp4064627 | J. Phys. Chem. B XXXX, XXX, XXX−XXX

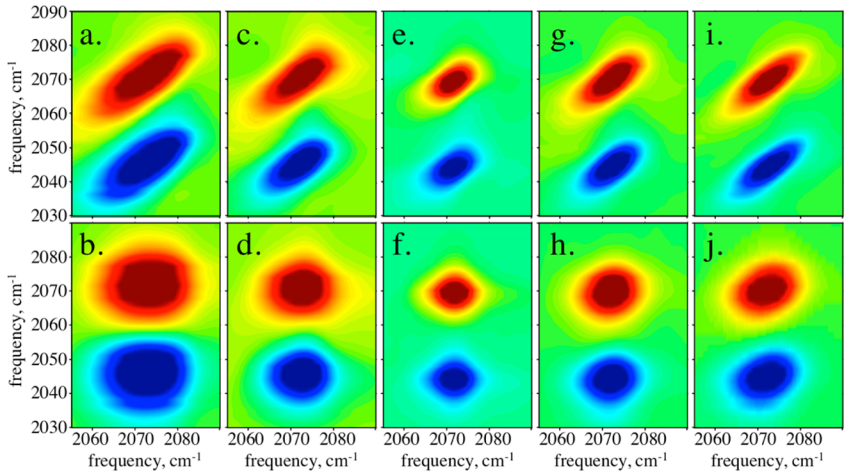

Figure 3. 2D-IR spectra collected at T_w = 0.3 (top row) and 30 ps (bottom row) for (a,b) neat $CHCl_3$, (c,d) 0.5 mol fraction $CHCl_3$ in d_6-benzene, (e,f) neat d_6-benzene, (g,h) 0.5 mol fraction BA in d_6-benzene, and (i,j) neat BA.

tions to the VC-I_2 carbonyl line shape for each of the binary solvent mixtures.

Figure 3e (top middle frame) shows the early T_w 2D-IR spectrum for d_6-benzene with characteristic diamond-shaped peaks that indicate that the line shape is primarily homogeneously broadened.[9,48] At this T_w, there is some elongation along the diagonal due to inhomogeneity, but the peaks become symmetric by 30 ps (Figure 3f) through spectral diffusion. Moving to the left, the d_6-benzene is progressively diluted with $CHCl_3$, and the line shapes become diagonally elongated. The dramatic broadening with increasing proportion of $CHCl_3$ shown in the FTIR spectra is reflected here. Qualitatively, the line shapes do not differ largely apart from the broadening and loss of the diamond shape. At 0.3 ps, the frequencies of the CO stretch during the initial and final coherences are strongly correlated with one another. By 30 ps, this is no longer the case; each of the lower spectra shows a rounded line shape. The same trend is observed moving to the right of the middle frames in Figure 3, diluting the d_6-benzene with a more polar solvent, though for BA, the broadening is more modest. In contrast to the $CHCl_3$ mixtures, there are clear dynamical differences shown in these spectra. Notice particularly that the peak is slightly thinner along the antidiagonal dimension in pure BA (Figure 3i) as opposed to the 0.5 mol fraction mixture (Figure 3g). Comparing short to long T_w's for binary mixtures of $CHCl_3$ (Figure 3a–d) to those of BA (Figure 3g–j) shows that all of the dynamics have been sampled by 30 ps in $CHCl_3$, whereas the BA samples remain visibly elongated along the diagonal. The $CHCl_3$ and d_6-benzene solvation dynamics have enabled all of the carbonyl oscillators on VC-I_2 to sample all of the available frequencies under the linear line shape by 30 ps, but in BA and BA/d_6-benzene mixtures, some oscillators still remain partially correlated with their starting frequencies.

In order to quantify the data, we used the CLS method outlined by Fayer and co-workers.[1,2] For a given 2D-IR spectrum, slices were taken parallel to the y-axis (ω_m) in Figure 3, and the positive-going maxima for the slices were identified by fitting to a peak function. These peak points were then connected to form a line that tracks the ridge maximum over the 0–1 transition. As T_w increased in the 2D-IR pulse sequence, the slope of this line evolved from a positive slope when the peak shape was elongated along the diagonal (e.g., Figure 3a) to a slope of zero when spectral diffusion was complete, and the band shape was horizontally symmetric (e.g., Figure 3b). The CLS decay is commonly modeled as a sum of exponential decays and has been rigorously shown to provide a normalized analogue of the FFCF.[1,2] The FFCF also includes a homogeneous term, which will be discussed below. In the limit of T_w = 0 (CLS y-intercept), deviations of the CLS from unity are the result of homogeneous broadening and very fast spectral diffusion. Using the linear spectrum, this normalized deviation can be used to determine the actual homogeneous line width and the unnormalized FFCF with amplitudes and time constants that are directly comparable to the results from MD simulations.[1,2,54,55]

It should be noted that a few of the linear line shapes for these samples were not well-fit by a single Gaussian peak, particularly those at higher mole fractions (≥0.5) of $CHCl_3$.[14] This can occur either when non-Gaussian dynamics are present or when multiple peaks with distinct dynamics overlap. Although the CLS method was derived using the assumption of Gaussian dynamics, it has been shown that it gives accurate values for the time constants even when applied to non-Gaussian systems.[56] It is also possible that the line shapes represent multiple modes in discrete environments with different dynamics, in which case the CLS decay would not perfectly correlate with the FFCF.[57] However, we did not observe off-diagonal peaks from coupling or exchange or a frequency dependence of the CLS decay over the majority of the line widths, which would be indicative of these scenarios (see the Supporting Information for representative spectra with CLS values overlaid).

Figure 4a and b shows the CLS values as a function of T_w overlaid with a multiexponential fit for both types of binary solvent mixtures. The markers represent a mean CLS measured for between three and six different 2D-IR spectra, and the error bars, which in many cases are smaller than the size of the markers, show the standard deviations from the mean. The solid lines are a multiexponential plus a constant fit to the complete set of values (not simply the mean), and it can be seen that the signal-to-noise ratio is very high and the fits are very good. The black curve in each frame shows the CLS decay in neat d_6-benzene, and it is clear that both $CHCl_3$ and BA have the effect of increasing the y-intercept. Consistent with the 2D-IR spectral observations in Figure 3, the $CHCl_3$ mixtures show

dx.doi.org/10.1021/jp4064627 | J. Phys. Chem. B XXXX, XXX, XXX–XXX

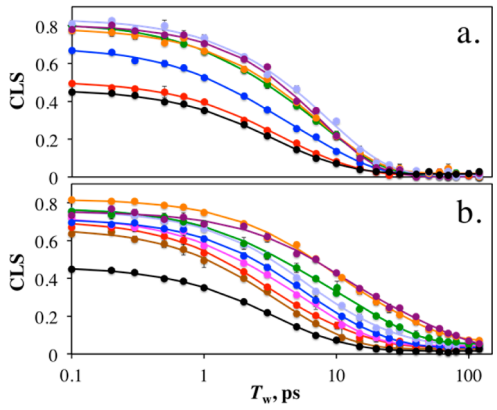

Figure 4. CLS decays as a function of T_w for binary mixtures of (a) 0 (black), 0.1 (red), 0.3 (blue), 0.5 (green), 0.7 (orange), 0.9 (lavender), and 1 (purple) mole fraction $CHCl_3$ in d_6-benzene and (b) 0 (black), 0.05 (brown), 0.1 (red), 0.2 (pink), 0.3 (blue), 0.4 (lavender), 0.5 (green), 0.7 (orange), and 1 (purple) mole fraction BA in d_6-benzene. Overlaid solid lines are the multiexponential fits to the data markers.

decays that reach their minimum values at similar times well before 50 ps. The BA mixtures take increasingly longer to decay, indicating that the dynamics are slower. The best-fit parameters to these decays are given in Table S1 in the Supporting Information. However, it is instructive to view these graphically to assess the dynamical trends.

The FFCF was modeled according to eq 2, except in the case of pure chloroform, where only the first two terms were necessary

$$\mathrm{FFCF}(t) = \frac{\delta(t)}{T_2} + {\Delta_1}^2 \exp\left(\frac{-t}{\tau_1}\right) + {\Delta_2}^2 \exp\left(\frac{-t}{\tau_2}\right) + {\Delta_0}^2 \quad (2)$$

The time constants (τ_1 and τ_2) in this equation were obtained directly from fitting the CLS decays in Figure 4, which has been shown to be highly accurate.[1,2] However, the amplitudes of each exponential contribution assume a FFCF normalized to unity, and the y-intercept is likewise normalized and may include contributions from very fast spectral diffusion. Following the procedure by Kwak and co-workers, the amplitudes from the fits to the CLS decays and the linear FWHMs were used to calculate approximate values for the unnormalized amplitudes (Δ_i) and T_2.[1,2] These starting values were then applied to a FFCF, and the first-order response function was used to reproduce the linear line shape. The amplitudes, as well as the central frequencies, were iteratively varied to fit the linear line shape. Only Δ values for those terms where the time constants were small compared with the free induction decay (FID, obtained from the Fourier transform of the linear spectrum) were allowed to float, where small is defined as less than five times the FID decay time. The CLS method was developed using the short-time approximation, which underestimates the values for Δ_i and T_2 due to the method's inability to distinguish between homogeneous terms and fast (compared with FID) spectral diffusion. Thus, the floated Δ_i and T_2 values were constrained to only increase from the estimated values. In all cases, the Δ_i values that were fit did not change from the initial guesses. The wings of the line shapes of the linear spectra in mixtures containing the majority of $CHCl_3$ did not fit well due to the asymmetry of the peak,[14,31] but the widths were well-reproduced. The full set of fit parameters, including the fitted center frequencies and T_2 values, are given in Table S2 in the Supporting Information. The final Δ_i and τ_i values that comprised the full FFCF are shown in Table 1. The homogeneous linewidths Γ were calculated from the T_2 values using eq 1 and are also included in Table 1. The errors on each parameter are included in parentheses as a single ($\pm$) value or independent positive and negative ($+/-$) values.

Figure 5 plots the time constants and Δ_i values of the exponential components of the determined FFCF. All decays were fit well with a biexponential (plus a constant offset) except for the neat $CHCl_3$, which was sufficiently modeled with a single exponential. Within error, the time constants for spectral diffusion are independent of the mole fraction of $CHCl_3$, having values of ~2 and ~8 ps in all mixtures. It is obligatory to state that connecting the time scales from the FFCF to microscopic events is not readily achieved with 2D-IR alone. What we can say is that the characteristic time scales for frequency

Table 1. FFCF Parameters for BA and $CHCl_3$ Binary Mixtures in d_6-Benzene

mole fraction	Δ_1 (rad/ps)	τ_1 (ps)	Δ_2 (rad/ps)	τ_2 (ps)	Δ_0 (rad/ps)	Γ (cm^{-1})
			$CHCl_3$ in Benzene-d_6			
0	0.47 (0.02/0.12)	2.4 (0.5)	0.41 (0.01/0.12)	7.0 (1.6)	0.12 (0.03/0.05)	2.3 (0.1/0.1)
0.1	0.44 (0.02/0.10)	2.0 (0.5)	0.57 (0.01/0.09)	6.8 (1.0)	0.10 (0.03/0.03)	1.9 (0.1/0.1)
0.3	0.49 (0.04/0.04)	1.5 (0.2)	0.68 (0.01/0.04)	8.0 (0.5)	0.10 (0.07/0.02)	2.3 (0.2/0.1)
0.5	0.42 (0.10/0.04)	1.4 (0.4)	0.86 (0.02/0.03)	8.6 (0.5)	0.10 (0.15/0.02)	2.2 (0.5/0.2)
0.7	0.36 (0.27/0.07)	1.6 (1.0)	1.03 (0.05/0.04)	8.1 (0.6)	0.17 (0.26/0.02)	1.9 (1.6/0.2)
0.9	0.38 (0.42/0.07)	1.6 (1.3)	1.20 (0.10/0.03)	9.3 (0.7)	0.13 (0.84/0.02)	2.1 (2.6/0.1)
1			1.34 (0.11/0.002)	7.7 (0.1)		2.2 (0.3/0.3)
			BA in d_6-Benzene			
0	0.47 (0.02/0.12)	2.4 (0.5)	0.41 (0.01/0.12)	7.0 (1.6)	0.12 (0.03/0.05)	2.3 (0.1/0.1)
0.05	0.39 (0.02/0.19)	1.8 (0.7)	0.53 (0.01/0.18)	5.9 (1.1)	0.14 (0.02/0.07)	2.5 (0.1/0.1)
0.1	0.5 (0.01/0.1)	2.2 (0.4)	0.47 (0.01/0.1)	9.6 (1.8)	0.16 (0.02/0.04)	2.2 (0.1/0.1)
0.2	0.35 (0.03/0.09)	1.4 (0.6)	0.62 (0.01/0.07)	7.6 (0.8)	0.18 (0.02/0.03)	1.9 (0.1/0.1)
0.3	0.52 (0.01/0.12)	3.6 (0.8)	0.56 (0.01/0.12)	12.3 (2.1)	0.17 (0.03/0.05)	1.6 (0.2/0.1)
0.4	0.56 (0.01/0.08)	4.2 (0.6)	0.53 (0.01/0.08)	15.9 (2.4)	0.21 (0.02/0.03)	1.6 (0.2/0.1)
0.5	0.45 (0.02/0.04)	2.6 (0.5)	0.66 (0.01/0.04)	16.8 (1.5)	0.22 (0.02/0.02)	1.5 (0.1/0.1)
0.7	0.53 (0.01/0.05)	5.6 (0.9)	0.62 (0.01/0.06)	26.8 (3.6)	0.25 (0.02/0.03)	0.9 (0.1/0.1)
1	0.62 (0.01/0.05)	7.5 (1.0)	0.65 (0.01/0.04)	45.4 (9.3)	0.18 (0.03/0.06)	0.7 (0.1/0.1)

dx.doi.org/10.1021/jp4064627 | J. Phys. Chem. B XXXX, XXX, XXX−XXX

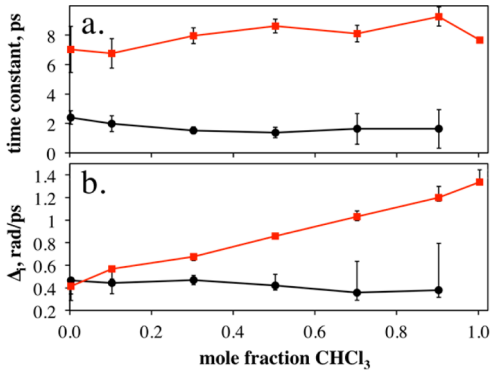

Figure 5. Graphical representation of full FFCF parameters for binary mixtures of $CHCl_3$ in d_6-benzene showing (a) the τ_1 (black circles) and τ_2 (red squares) and (b) Δ_1 (black circles) and Δ_2 (red squares). Error bars in (a) represent the standard error of the fit. Positive error bars in (b) show the range of values for which the FTIR line shape is fit 98% as well as the best value. Because the amplitudes were constrained positively (see text), the negative error bars in (b) represent the propagated error of the CLS fits.

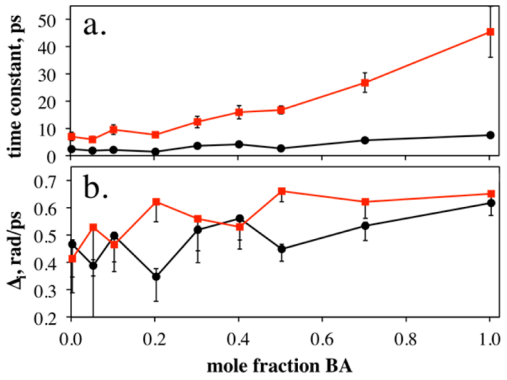

Figure 6. Graphical representation of full FFCF parameters for binary mixtures of BA in d_6-benzene showing (a) the τ_1 (black circles) and τ_2 (red squares) and (b) Δ_1 (black circles) and Δ_2 (red squares). Error bars in (a) represent the standard error of the fit. Positive error bars in (b) show the range of values for which the FTIR line shape is fit 98% as well as the best value. Because the amplitudes were constrained positively (see text), the negative error bars in (b) represent the propagated error of the CLS fits.

decorrelation, regardless of their molecular origins, are unaffected by changing the $CHCl_3/d_6$-benzene composition. The Δ_i values (Figure 5b), however, show that there is a steady increase in the magnitude of the ~8 ps dynamics, while the ~2 ps dynamic contribution diminishes and vanishes in neat $CHCl_3$. Conceptually, the Δ_i values indicate the magnitude of the frequency fluctuations that are being modulated on a time scale of τ_i. With no changes in the time scale of a dynamical process, increasing Δ leads to faster decorrelation of vibrational modes in the ensemble, a faster FID, and therefore a broader linear line shape. Taken together, these two frames paint a picture of spectral diffusion that is driven by two dominant processes in d_6-benzene, perhaps a molecular motion in VC-I_2 that modulates the carbonyl frequency and is coupled to the solvent shell and a proximal solvent motion that more directly affects the CO mode. Although this is conjecture in the absence of corroborating simulations, Figure 5a and b might then show the change in the intramolecular potential in the former case with additional $CHCl_3$ and the loss of the latter contribution as d_6-benzene is progressively diluted and replaced with $CHCl_3$ in the solvation shell. Within the error bars of these measurements, the Δ_i values change in an effectively linear fashion with mole fraction, but it can be seen in Figure 5a that the longer time constants of spectral diffusion show a slight increase up to about the 0.5 mol fraction before leveling off. Here, we see that the time constants for spectral diffusion are the only parameters in the FFCF that show any correlation with the change in the rate of broadening in Figure 2. It is a minor effect, but the time constant getting slightly longer would cause the rate of broadening to be somewhat slower up to 0.5 mol fraction.

The dynamical behavior is notably different when d_6-benzene is diluted instead with the more polar BA, which we believe to preferentially solvate VC-I_2 over benzene. Figure 6a and b shows the τ and Δ values of the FFCF. The time constants increase progressively, while the magnitudes of the frequency fluctuations are anticorrelated and show very minor changes with the mole fraction of BA. In comparison to the $CHCl_3$ mixtures, it can be said that the time scales of CO decorrelation progressively become much slower from ~2 and ~8 ps in neat d_6-benzene to ~8 and ~45 ps, respectively, in neat BA. Furthermore, both time constants only begin to increase significantly beginning at around 0.2 mol fraction, the approximate area where the linear FWHM changed its slope (see Figure 2). This is accompanied by a mild nonlinear increase in the Δ_2 value in this same range in Figure 6b, indicating that while this process is becoming characteristically slower, the magnitudes of the frequency fluctuations become larger. Thus, we can see in this graphical representation of the FFCF parameters that there is nonlinear behavior in the spectral diffusion with the mole fraction of BA, showing that preferential solvation of VC-I_2 by BA over d_6-benzene leads to corresponding changes in the inhomogeneous dynamics.

The final piece in this spectral broadening puzzle is to consider the homogeneous contribution to the line width across both binary solvent mixtures. Figure 7 shows the

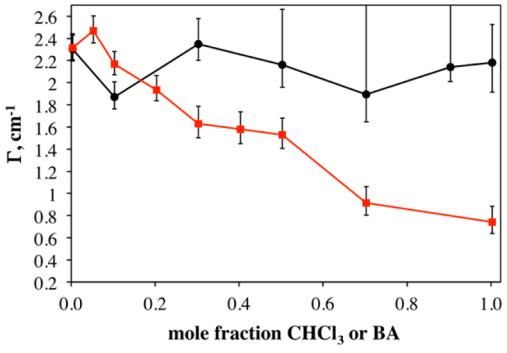

Figure 7. Homogeneous line width (Γ, cm^{-1}) as a function of mole fraction for $CHCl_3$ (black) and BA (red) mixtures. Error bars represent the range of values for which the FTIR line shape is fit 99% as well as the best value (except where noted in Table 1).

homogeneous line width as calculated from T_2 for both sets of mixtures ($CHCl_3$ = black circles; BA = red squares) as a function of mole fraction. The values are typically on the order of a few wavenumbers. Considering the T_1 and T_{orient} contributions as they were calculated above, this demonstrates that the T_2^* contribution is dominant. Intriguingly, the $CHCl_3$ mixtures show virtually no change in Γ as the d_6-benzene is diluted with $CHCl_3$, despite the fact that the linear line width more than doubles! This reveals that this enormous and

dx.doi.org/10.1021/jp4064627 | J. Phys. Chem. B XXXX, XXX, XXX−XXX

dramatic broadening shown in the FTIR is almost entirely due to an increase in the variety of solvation environments and spectral diffusion. Because the time constants also remain nearly the same for this system over the entire range of solvent compositions, the most significant source of this inhomogeneous broadening (apart from the natural increase in the number of environments that occurs when adding a more polar solvent) is the increase in Δ_1, the magnitude of the frequency shifts for the slow spectral diffusion component. Closer examination of the FFCF parameters shows that there is also a corresponding small increase in the FFCF constant offset with mole fraction, showing that the increase in inhomogeneous broadening also includes some slow unresolved processes (see the Supporting Information).

In contrast, the Γ for the BA mixtures shows considerable decrease throughout the range of solvent compositions from a value of ~2.3 cm^{-1} in pure d_6-benzene to ~0.7 cm^{-1} in pure BA. This is again consistent with the observations made concerning the 2D-IR spectra of the BA mixtures that the pure BA sample had a visibly thinner line shape at the short T_w's. Considering that the FTIR line width increases by almost half, this is also a striking result. Again, the increased broadening is certainly not coming from the homogeneous line width but rather from inhomogeneous broadening. The increase in the characteristic time scales of spectral diffusion shown in Figure 6a would narrow the line shape rather than broadening it, but this could be counteracted by increases in Δ. Therefore, we must conclude that the nonlinear increase in line width up to 0.2 mol fraction of BA cannot be the result of homogeneous broadening. Furthermore, the intuitive expectation that a more polar solvent should lead to greater inhomogeneous contributions is recovered, despite a narrower linear line shape in BA versus $CHCl_3$, because the BA induces a decrease in Γ that counters the increase in inhomogeneity.

CONCLUSIONS

Despite a lack of solvatochromism,[14,31] the linear line width of the carbonyl on VC-I_2 varies dramatically and nonlinearly when d_6-benzene is systematically replaced by $CHCl_3$ or BA. The broadening is more pronounced in $CHCl_3$, which is surprising considering that BA is more polar. Herein, we have used FTIR and 2D-IR spectroscopies to tease apart the major contributing factors to these line shapes, in the process establishing the full FFCF for this vibration across a range of binary mixed solvents. With this information, the homogeneous and inhomogeneous broadening contributions are determined. The primary contributor to the homogeneous line width is pure dephasing for VC-I_2, and we have shown that this contribution is unchanged across all mixtures of $CHCl_3$ in d_6-benzene while decreasing significantly for BA mixtures. This demonstrates that the gains in linear line width in both cases must have their origins in inhomogeneous contributions.

Using CLS decay analysis, we characterized the inhomogeneous broadening as well. The BA mixtures have much slower characteristic time scales for spectral diffusion than are present in d_6-benzene or any of the $CHCl_3$ mixtures. BA is about 10 times more viscous than $CHCl_3$ or d_6-benzene, it is known to be a relatively strong hydrogen bond donor, and its higher dipole moment certainly strengthens the interactions with VC-I_2, and any of these factors could explain the slowed dynamics. Yet, slower time constants in the FFCF generally lead to line shape narrowing, and therefore, these temporal differences cannot be the reason for spectral broadening. The explanation lies in the corresponding increases in the magnitudes of the frequency fluctuations in the FFCF that correlate with the preferential solvation profile of the line shapes in both types of solvent mixtures with mole fraction. Furthermore, ignoring contributions from spectral diffusion to the line width and simply taking the ratio of the linear FWHM to the homogeneous line width in each neat solvent, we obtain a value for d_6-benzene of 3.5, for chloroform of 7.4, and for benzyl alcohol of 15.5. This trend, unlike that of the absolute FTIR width, is consistent with that expected for these solvents considering their relative dipole moments.

Overall, we have taken the vibrational mode on the adduct of a model catalyst and applied an in-depth evaluation of the origins of spectral broadening. Our results show how straightforward analysis of 2D-IR line shapes can be used to uncover otherwise lost dynamical information about the solvation dynamics. A natural extension of these experiments would be to investigate the influence of changing the trans ligand to one that is perhaps more sensitive to its solvation environment in order to determine whether the dynamics sensed by the reporter reflect the active site of the catalyst. Experimental directions of this type are underway in our laboratories at this time.

ASSOCIATED CONTENT

Supporting Information

2D-IR spectra for VC-I_2 in all binary solvent mixtures at all T_w's. Best-fit multiexponential parameters for CLS decays in all solvent mixtures. Best-fit parameters to optimize the dynamic amplitudes and T_2 starting with CLS parameters. Selected 2D-IR spectra with overlaid CLS values. This material is available free of charge via the Internet at http://pubs.acs.org.

AUTHOR INFORMATION

Notes

The authors declare no competing financial interest.

ACKNOWLEDGMENTS

The authors gratefully acknowledge funding from the National Science Foundation under CHE-0847356.

REFERENCES

(1) Kwak, K.; Park, S.; Finkelstein, I. J.; Fayer, M. D. Frequency–Frequency Correlation Functions and Apodization in Two-Dimensional Infrared Vibrational Echo Spectroscopy: A New Approach. *J. Chem. Phys.* **2007**, *127* (12), 124503.

(2) Kwak, K.; Rosenfeld, D. E.; Fayer, M. D. Taking Apart the Two-Dimensional Infrared Vibrational Echo Spectra: More Information and Elimination of Distortions. *J. Chem. Phys.* **2008**, *128* (20), 204505.

(3) Oxtoby, D. W. Vibrational-Relaxation in Liquids. *Annu. Rev. Phys. Chem.* **1981**, *32*, 77–101.

(4) Schweizer, K. S.; Chandler, D. Vibrational Dephasing and Frequency-Shifts of Polyatomic-Molecules in Solution. *J. Chem. Phys.* **1982**, *76* (5), 2296–2314.

(5) Tan, H. S.; Piletic, I. R.; Fayer, M. D. Orientational Dynamics of Water Confined on a Nanometer Length Scale in Reverse Micelles. *J. Chem. Phys.* **2005**, *122* (17), 057405.

(6) Tan, H. S.; Piletic, I. R.; Fayer, M. D. Polarization Selective Spectroscopy Experiments: Methodology and Pitfalls. *J. Opt. Soc. Am. B* **2005**, *22* (9), 2009–2017.

(7) Eigner, A. A.; Anglin, T. C.; Massari, A. M. 2D-IR Studies of Annealing-Induced Changes to Structural Dynamics in Organic Semiconductor Thin Films. *J. Phys. Chem. C* **2010**, *114* (28), 12308–12315.

(8) Jones, B. H.; Huber, C. J.; Massari, A. M. Solvation Dynamics of Vaska's Complex by 2D-IR Spectroscopy. *J. Phys. Chem. C* **2011**, *115* (50), 24813−24822.
(9) Khalil, M.; Demirdoven, N.; Tokmakoff, A. Coherent 2D IR Spectroscopy: Molecular Structure and Dynamics in Solution. *J. Phys. Chem. A* **2003**, *107* (27), 5258−5279.
(10) Kolano, C.; Helbing, J.; Kozinski, M.; Sander, W.; Hamm, P. Watching Hydrogen-Bond Dynamics in a Beta-Turn by Transient Two-Dimensional Infrared Spectroscopy. *Nature* **2006**, *444* (7118), 469−472.
(11) Nydegger, M. W.; Dutta, S.; Cheatum, C. M. Two-Dimensional Infrared Study of 3-Azidopyridine As a Potential Spectroscopic Reporter of Protonation State. *J. Chem. Phys.* **2010**, *133* (13), 134506.
(12) Shim, S. H.; Strasfeld, D. B.; Ling, Y. L.; Zanni, M. T. Automated 2D IR Spectroscopy Using a Mid-IR Pulse Shaper and Application of This Technology to the Human Islet Amyloid Polypeptide. *Proc. Natl. Acad. Sci. U.S.A.* **2007**, *104* (36), 14197−14202.
(13) Park, S.; Kwak, K.; Fayer, M. D. Ultrafast 2D-IR Vibrational Echo Spectroscopy: A Probe of Molecular Dynamics. *Laser Phys. Lett.* **2007**, *4* (10), 704−718.
(14) Jones, B. H.; Huber, C. J.; Massari, A. M. Solvent-Mediated Vibrational Energy Relaxation from Vaska's Complex Adducts in Binary Solvent Mixtures. *J. Phys. Chem. A* **2013**, *117* (29), 6150−6157.
(15) Vaska, L.; Chen, L.; Senoff, C. Oxygen-Carrying Iridium Complexes: Kinetics, Mechanism, And Thermodynamics. *Science* **1971**, *174* (4009), 587−589.
(16) Vaska, L.; Rhodes, R. E. Homogeneous Catalytic Hydrogenation of Ethylene and Acetylene with Four-Coordinated Iridium and Rhodium Complexes. Reversible Catalyst-Substrate Adducts1. *J. Am. Chem. Soc.* **1965**, *87* (21), 4970−4971.
(17) Vaska, L.; Tadros, M. Catalytic Hydrogenolysis of Molecular Oxygen by Transition Metal Complexes in Nonaqueous Solution. *J. Am. Chem. Soc.* **1971**, *93*, 7099−7101.
(18) Vaska, L. Reversible Activation of Covalent Molecules by Transition-Metal Complexes. The Role of the Covalent Molecule. *Acc. Chem. Res.* **1968**, *1* (11), 335−344.
(19) Atwood, J. Organoiridium Complexes as Models for Homogeneously Catalyzed Reactions. *Coord. Chem. Rev.* **1988**, *83*, 93−114.
(20) La Placa, S.; Ibers, J. Structure of $IrO_2Cl(CO)(P(C_6H_5)_3)_2$, the Oxygen Adduct of a Synthetic Reversible Molecular Oxygen Carrier1. *J. Am. Chem. Soc.* **1965**, *87*, 2581−2586.
(21) Chock, P. B.; Halpern, J. Kinetics of the Addition of Hydrogen, Oxygen, and Methyl Iodide to Some Square-Planar Iridium (I) Complexes. *J. Am. Chem. Soc.* **1966**, *88* (15), 3511−3514.
(22) Margl, P.; Ziegler, T.; Bloechl, P. Reaction of Methane with $Rh(PH_3)_2Cl$: A Dynamical Density Functional Study. *J. Am. Chem. Soc.* **1995**, *117*, 12625−12634.
(23) Margl, P.; Ziegler, T.; Bloechl, P. Migratory CO Insertion and Aldehyde Formation in Carbonylation of Methane by the $Rh(PH_3)_2Cl$ Catalyst. A Dynamical Density Functional Study. *J. Am. Chem. Soc.* **1996**, *118*, 5412−5419.
(24) P'Pool, S.; Klingshirn, M.; Rogers, R.; Shaughnessy, K. Kinetic Study of the Oxidative Addition of Methyl Iodide to Vaska's Complex in Ionic Liquids. *J. Organomet. Chem.* **2005**, *690*, 3522−3528.
(25) Selke, M.; Foote, C. Reactions of Organometallic Complexes with Singlet Oxygen. Photooxidation of Vaska's Complex. *J. Am. Chem. Soc.* **1993**, *115*, 1166−1167.
(26) Stang, P. J.; Schiavelli, M. D.; Chenault, H. K.; Breidegam, J. L. Kinetic Deuterium Isotope Effects in the Reaction of Vaska's Compound $(Ph_3P)_2Ir(CO)Cl$ with CH_3I and $CH_3OSO_2CF_3$. *Organometallics* **1984**, *3*, 1133−1134.
(27) Thompson, W.; Sears, C., Jr. Kinetics of Oxidative Addition to Iridium(I) Complexes. *Inorg. Chem.* **1977**, *16*, 769−774.
(28) Zahalka, H. A.; Alper, H.; Sasson, Y. Homogeneous Decarbonylation of Formate Esters Catalyzed by Vaska's Compound. *Organometallics* **1986**, *5*, 2497−2499.
(29) Cotton, F. A. *Advanced Inorganic Chemistry*, 5th ed.; Wiley-Interscience, Inc.: New York, 1988.
(30) Ray, G. B.; Li, X. Y.; Ibers, J. A.; Sessler, J. L.; Spiro, T. G. How Far Can Proteins Bend the FeCO Unit: Distal Polar and Steric Effects in Heme-Proteins and Models. *J. Am. Chem. Soc.* **1994**, *116* (1), 162−176.
(31) Huber, C. J.; Anglin, T. C.; Jones, B. H.; Muthu, N.; Cramer, C. J.; Massari, A. M. Vibrational Solvatochromism in Vaska's Complex Adducts. *J. Phys. Chem. A* **2012**, *116* (37), 9279−9286.
(32) Cichos, F.; Willert, A.; Rempel, U.; Von Borczyskowski, C. Solvation Dynamics in Mixtures of Polar and Nonpolar Solvents. *J. Phys. Chem. A* **1997**, *101* (44), 8179−8185.
(33) Luther, B.; Kimmel, J.; Levinger, N. Dynamics of Polar Solvation in Acetonitrile−Benzene Binary Mixtures: Role of Dipolar and Quadrupolar Contributions to Solvation. *J. Chem. Phys.* **2002**, *116* (8), 3370−3377.
(34) Nguyen, C. N.; Stratt, R. M. Preferential Solvation Dynamics in Liquids: How Geodesic Pathways through the Potential Energy Landscape Reveal Mechanistic Details about Solute Relaxation in Liquids. *J. Chem. Phys.* **2010**, *133* (12), 124503.
(35) Aagaard, O. M.; Meier, R. J.; Buda, F. Ruthenium-Catalyzed Olefin Metathesis: A Quantum Molecular Dynamics Study. *J. Am. Chem. Soc.* **1998**, *120* (29), 7174−7182.
(36) Bianco, R.; Hay, P. J.; Hynes, J. T. Theoretical Study of O−O Single Bond Formation in the Oxidation of Water by the Ruthenium Blue Dimer. *J. Phys. Chem. A* **2011**, *115* (27), 8003−8016.
(37) Caratzoulas, S.; Vlachos, D. G. Converting Fructose to 5-Hydroxymethylfurfural: A Quantum Mechanics/Molecular Mechanics Study of the Mechanism and Energetics. *Carbohydr. Res.* **2011**, *346* (5), 664−672.
(38) Ensing, B.; Meijer, E. J.; Blochl, P. E.; Baerends, E. J. Solvation Effects on the S_N2 Reaction between CH_3Cl and Cl^- in Water. *J. Phys. Chem. A* **2001**, *105* (13), 3300−3310.
(39) Grossman, M.; Born, B.; Heyden, M.; Tworowski, D.; Fields, G. B.; Sagi, I.; Havenith, M. Correlated Structural Kinetics and Retarded Solvent Dynamics at the Metalloprotease Active Site. *Nat. Struct. Mol. Biol.* **2011**, *18*, 1102−1108.
(40) Handgraaf, J. W.; Meijer, E. J. Realistic Modeling of Ruthenium-Catalyzed Transfer Hydrogenation. *J. Am. Chem. Soc.* **2007**, *129* (11), 3099−3103.
(41) Wang, L. P.; Wu, Q.; Van Voorhis, T. Acid−Base Mechanism for Ruthenium Water Oxidation Catalysts. *Inorg. Chem.* **2010**, *49* (10), 4543−4553.
(42) Faeder, S. M. G.; Jonas, D. M. Two-Dimensional Electronic Correlation and Relaxation Spectra: Theory and Model Calculations. *J. Phys. Chem. A* **1999**, *103* (49), 10489−10505.
(43) Eckbreth, A. C. Boxcars — Crossed-Beam Phase-Matched Cars Generation in Gases. *Appl. Phys. Lett.* **1978**, *32* (7), 421−423.
(44) Fayer, M. D. Fast Protein Dynamics Probed with Infrared Vibrational Echo Experiments. *Annu. Rev. Phys. Chem.* **2001**, *52*, 315−356.
(45) Fayer, M. D. Dynamics of Liquids, Molecules, and Proteins Measured with Ultrafast 2D IR Vibrational Echo Chemical Exchange Spectroscopy. *Annu. Rev. Phys. Chem.* **2009**, *60*, 21−38.
(46) Hamm, P.; Hochstrasser, R. M. Structure and Dynamics of Proteins and Peptides: Femtosecond Two-Dimensional Infrared Spectroscopy. In *Ultrafast Infrared and Raman Spectroscopy*; Fayer, M. D., Ed.; Marcel Dekker, Inc.: New York, 2001; Vol. *26*, pp 273−347.
(47) Massari, A. M.; Finkelstein, I. J.; McClain, B. L.; Goj, A.; Wen, X.; Bren, K. L.; Loring, R. F.; Fayer, M. D. The Influence of Aqueous vs Glassy Solvents on Protein Dynamics: Vibrational Echo Experiments and Molecular Dynamics Simulations. *J. Am. Chem. Soc.* **2005**, *127*, 14279−14289.
(48) Khalil, M.; Demirdoven, N.; Tokmakoff, A. Obtaining Absorptive Line Shapes in Two-Dimensional Infrared Vibrational Correlation Spectra. *Phys. Rev. Lett.* **2003**, *90* (4), 047401.
(49) Asbury, J. B.; Steinel, T.; Kwak, K.; Corcelli, S. A.; Lawrence, C. P.; Skinner, J. L.; Fayer, M. D. Dynamics of Water Probed with

Vibrational Echo Correlation Spectroscopy. *J. Chem. Phys.* **2004**, *121* (24), 12431−12446.
(50) El Seoud, O. A. Solvation in Pure and Mixed Solvents: Some Recent Developments. *Pure Appl. Chem.* **2007**, *79* (6), 1135−1151.
(51) Silva, P. L.; Trassi, M. A. S.; Martins, C. T.; El Seoud, O. A. Solvatochromism in Binary Mixtures: First Report on a Solvation Free Energy Relationship between Solvent Exchange Equilibrium Constants and the Properties of the Medium. *J. Phys. Chem. B* **2009**, *113* (28), 9512−9519.
(52) Benamotz, D.; Scott, T. W. Microscopic Frictional Forces on Molecular-Motion in Liquids — Picosecond Rotational Diffusion in Alkanes and Alcohols. *J. Chem. Phys.* **1987**, *87* (7), 3739−3748.
(53) Spears, K. G.; Cramer, L. E. Rotational Diffusion in Aprotic and Protic Solvents. *Chem. Phys.* **1978**, *30* (1), 1−8.
(54) Merchant, K. A.; Noid, W. G.; Akiyama, R.; Finkelstein, I. J.; Goun, A.; McClain, B. L.; Loring, R. F.; Fayer, M. D. Myoglobin−CO Substate Structures and Dynamics: Multidimensional Vibrational Echoes and Molecular Dynamics Simulations. *J. Am. Chem. Soc.* **2003**, *125* (45), 13804−13818.
(55) Bakulin, A. A.; Liang, C.; Jansen, T. L.; Wiersma, D. A.; Bakker, H. J.; Pshenichnikov, M. S. Hydrophobic Solvation: A 2D IR Spectroscopic Inquest. *Acc. Chem. Res.* **2009**, *42* (9), 1229−1238.
(56) Roy, S.; Pshenichnikov, M. S.; Jansen, T. L. C. Analysis of 2D CS Spectra for Systems with Non-Gaussian Dynamics. *J. Phys. Chem. B* **2011**, *115*, 5431−5440.
(57) Fenn, E. E.; Fayer, M. D. Extracting 2D IR Frequency−Frequency Correlation Functions from Two-Component Systems. *J. Chem. Phys.* **2011**, *135*, 074502.